Aggregation study of Brownian nanoparticles in convective phenomena

Mostafa Mahdavi[1], Mohsen Sharifpur[1,*], Mohammad H. Ahmadi[2,*] and Josua P. Meyer[1]

[1]Department of Mechanical and Aeronautical Engineering, University of Pretoria, Pretoria, 0028, South Africa
[2]Faculty of Mechanical Engineering, Shahrood University of Technology, Shahrood, Iran

*Correspondence to Mohsen Sharifpur (mohsen.sharifpur@up.ac.za) or Mohammad H. Ahmadi (mohammadhosein.ahmadi@gmail.com)

Abstract

The explanation of abnormal enhancement of transported energy in colloidal nanoparticles in a liquid has sparked much interest in recent years. The complexity comes from the inter-particle phenomenon and cluster formation. The process of nanoparticle aggregation, which is caused by convective phenomena and particle-to-particle interaction energy in a flow, is investigated in this research. Therefore, the probability of collision and cohesion among clusters is modelled, as stated in this research. ANSYS-Fluent 17 CFD tools are employed to implement a new method of nanoparticle aggregation, new essential forces, new heat law and cluster drag coefficient. The importance of the interaction forces is compared to drag force, and essential forces are considered in coupling between nanoparticles and fluid flow. An important parameter is defined for the surface energy density regarding the attractive energy between the double layer and surrounding fluid to capture the cohesion of particles. Particles' random migration is also presented through their angular and radial displacement. The analyses for interactions show the significance of Brownian motion in both particles' migration and coupling effects in the fluid. However, nanoparticles are pushed away from walls due to repulsive forces, and Brownian motion is found to be effective mainly on angular displacement around the tube centreline. The attractive energy is found to be dominant when two clusters are at an equal distance. Hence, the cluster formation in convective regions should be taken into account for modelling purposes. A higher concentrated region also occurs midway between the centreline and the heated wall.

Keywords Nanoparticles · Aggregation · Brownian motion · Cohesion · Surface energy · CFD

List of symbols

A	Hamaker constant (J)
A_p	Particle surface area (m^2)
A_{pp}	Particle projected area (m^2)
C_c	Cunningham correction factor
C_D	Drag coefficient
C_{ML}	Rotational coefficient
C_ω	Rotational drag coefficient
c_p	Specific heat (J kg^{-1} K^{-1})
d_p	Particle diameter (m)
D_T	Thermophoresis coefficient
f_{B_i}	Brownian force (N kg^{-1})
f_s	Interaction forces (N m^{-3})
f_d	Drag function
G_w	Gaussian weight function
h	Particle–particle distance (m)
I_p	Moment of inertia (kg m^{-2})
k	Thermal conductivity (W m^{-1} K^{-1})
K_B	Boltzmann constant (m^2 kg K^{-1} s^{-2})
m_p	Particle mass (kg)
$\dot{m}_p$	Particle mass flow rate (kg s^{-1})
$N_{particle}$	Number of particles in the parcel
n	Possible number of collision
P	Poisson distribution
Re_p	Particle Reynolds number
S_h	Thermal interaction between particles and fluid (W m^{-3})
Δt_p	Particle time step (s)
U_1, U_2	Uniform random number
u_p	Particle velocity (m s^{-1})

u_s	Particle–fluid relative velocity (m s^{-1})
V_{EDL}	Electric double-layer energy (J)
V_{vdw}	van der Waals energy (J)
x	Location (m)
Δx	Characteristic length of the cell
We	Webber number

Greek letters

ε_0	Vacuum permittivity (CV^{-1} m^{-1})
ε_r	Relative permittivity
κ	Debye–Huckel parameter (m^{-1})
γ	Surface energy density (J m^{-2})
$\dot{\gamma}$	Shear rate (1/s)
$\boldsymbol{\omega}_p$	Particle angular velocity (1/s)
$\boldsymbol{\Omega}$	Relative particle–liquid angular velocity (1/s)
ψ	Potential on the surface of particle (V)
$\theta_{particle}$	Particle variable in the node
$\bar{\theta}_{parcel}$	Particle variables affected by nodes in the neighbourhood
τ	Particle relaxation time (s)
$\bar{\zeta}$	Random function
χ	Random number between 0 and 1

Introduction

Nanoparticles have been used in some areas of industry in recent years due to their positive effect on heat transfer enhancement [1–3]. Both experimental and theoretical analyses have shown the increased thermal conductivity and viscosity of nanofluids [4–8]. Although both enhancement and deterioration in heat transfer coefficient or Nusselt number were reported by Yu et al. [9], the changes in viscosity are clearly caused by the interaction forces between solid and liquid. Some of the hypotheses behind the improved thermal conductivity are extensively explained by Aybar et al. [10]. The early assumption of the interaction of nanoparticles was indicated to be only thermophoresis and concentration diffusions, and has repeatedly been referred to by many researchers [11–15]. Krishnamurthy et al. [16] showed that the expanded mass diffusion of nanoparticles due to Brownian motion could be connected to thermal conductivity. Even though aggregation was mentioned as one of the contributing factors in this regard, as strongly suggested by Ganguly et al. [17], other researchers (Gupta and Kumar [18], Gharagozloo et al. [19] and Veilleux and Coulombe [20]) have emphasised that the random motion of the nanoparticles caused by Brownian motion was the reason for the diffusion. Putnam and Cahill [21] stated that thermo-diffusion depends mainly on the chemical characteristics of the particle surface and diameter, namely the ionic strength. Therefore, the changes in double-layer thickness (somehow represented by Debye length) and the pH of the mixture play an important role in the interaction of the nanoparticles. Eslamian and Saghir [22] discussed the non-equilibrium thermodynamics of thermophoresis coefficient for nanoparticles smaller than 2 nm. The coefficient was derived from the Brownian motion components and was found to be less than in previous studies [23, 24]. Koo and Kleinstreuer [25] assumed the thermal Brownian and van der Waals attraction forces as the contributing factors in added thermal conductivity. They stated that the flocculation in nanoparticles was unavoidable and it deteriorated in the case of metallic or metal oxide particles with higher kinetic energy than an electrostatic barrier. Vladkov and Barrat [26] simply assumed the Stokesian flow over the spherical nanoparticles (or equivalent diameter), with small and negligible flow convective terms. In fact, the transient and flow conduction passed over the particles were only considered in heat transfer equation. They modelled Kapitza resistance in the heat balance equation of a particle as the main thermal barrier. Gao et al. [27] hypothesised that the Brownian force and clustering of nanoparticles might be behind the abnormal enhancement of heat transfer. They eventually pointed out that the only significant phenomenon can be clustering and should be definitely considered in simulations. The same was reported by Babaei et al. [28] about Brownian force with different viewpoint using molecular dynamics simulations. Laín and Sommerfeld [29] used drag, gravity, lift and rotational forces for microscale particles in a turbulent flow. The collision among particles (and not cohesion which can be the dominant case in nanoscale) was considered important in the final distribution of particles. Anomalous diffusion in alumina nanofluid mixed with water, methanol and fluorometric dye for tracing was studied in a laminar microchannel flow by Ozturk et al. [30]. It was observed that the presence of surfactant and nanoparticles change the diffusion of fluorescence dye, meaning the changes in wettability and surface tension over the nanoparticles. They reported that the thermal conductivity was not considerably affected by the dye and surfactant comparing to the variation of diffusion rate. The changes in surface tension trend in a nanofluid with and without surfactant were also explained by Kumar and Milanova [31] and found to be higher with a surfactant. Moghari et al. [32] used mixture approach without considering any of the important slip mechanisms involved. Yang et al. [33] considered four mechanisms for mass diffusion of nanoparticles including gradients due to concentration, temperature, viscosity and shear-induced diffusion. Eventually, gradients due to concentration and temperature were found dominant comparing to others.

Literature review shows that researchers investigated the involved interactions among nanoparticles and also clusters in many reports separately, and only few reported the importance of each interaction or the combination of them. Therefore, it is crucial to explore the impacts of most of the phenomena involved with considering the corrections in correlations for particles cluster and Brownian motion. In this study, the attempt will be made to consider a variety of phenomena involved in nanoparticles migration and aggregation, as some of them mentioned above. The modifications in the model are implemented through some user-defined programs. The literature review shows that the following phenomena should be considered in nanoscale particles interactions: drag force, gravity, lift force, the force due to rotation or Magnus force, electrostatic attraction and repulsion forces, convective heat phenomenon around a particle, and the most importantly thermophoresis and random Brownian force. The possibility of particles collision and formation of clusters is also implemented.

Methodology and equations

A new development of nanoparticles migration and heat transfer in conjunction with Langevin equation is presented. The experiment results were borrowed from the work done by Zhang et al. [34] in a microchannel with 0.5 mm in diameter to validate the accuracy of the presented model. They used alumina nanoparticles with 20 nm average size and concentration from 0.25 to 0.77 vol%. The nanoparticles in the injection plan are released and tracked in the microchannel. The nanoparticles are initially assumed to be in uniform sizes, but changes in distribution and aggregation will occur during convective and diffusion migration. Before explanation of the equations, some early calculations were made to understand the importance of some forces. It was found out the pressure gradient, virtual mass and buoyancy forces can be safely neglected in calculations. Figure 1 presents the order of magnitude of each interaction comparing to drag force in each Cartesian direction. Z axis is the flow direction, and X and Y are the cross sections of the circular microchannel.

Since Brownian random force acts in all directions, the magnitude is considerable in three axes except in Z direction due to main drag direction. The repulsive electrical double-layer force (EDL) is also comparable to Brownian motion. It is noted that higher value of EDL means higher repulsion among nanoparticles and stability of the mixture. The contribution of lift, Magnus, van der Waals (vdw) and thermophoresis might be small, but still cannot be ignored and may have some influences on final aggregation of nanoparticles. With these simplifications, the nanoparticles

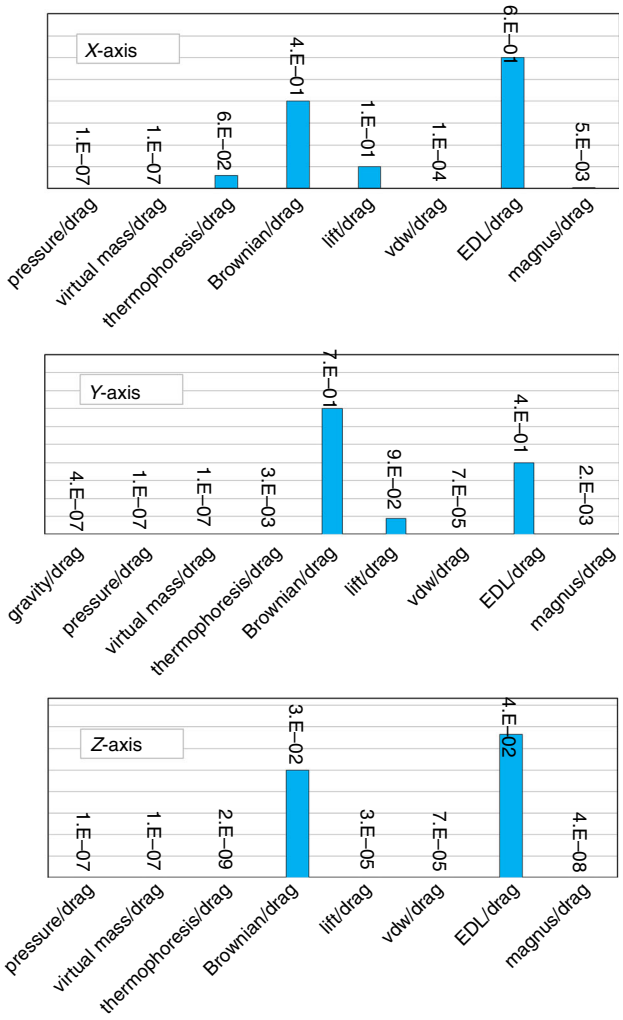

Fig. 1 Comparative study of interactions over nanoparticles

equations can be arranged without considering insignificant forces.

The simple form of continuity, momentum and energy equations is as follows:

$$\nabla.\left(\rho\vec{u}_{\mathrm{s}}\right) = 0, \tag{1}$$

$$\nabla\cdot\left(\rho\vec{u}_{\mathrm{s}}\vec{u}_{\mathrm{s}}\right) = -\nabla P + \nabla\cdot\left(\mu\nabla\vec{u}_{\mathrm{s}}\right) + f_{\mathrm{s}}, \tag{2}$$

$$\nabla\cdot\left(\rho\vec{u}_{\mathrm{s}}c_{\mathrm{p_c}}T_{\mathrm{c}}\right) = \nabla\cdot\left(k_{\mathrm{c}}\nabla T_{\mathrm{c}}\right) + S_{\mathrm{h}}. \tag{3}$$

The impacts of nanoparticles are seen in fluid equations through source terms f_{s} and S_{h}.

$$f_{\mathrm{s}} = \sum\left(\frac{18\mu_{\mathrm{c}}}{\rho_{\mathrm{p}}d_{\mathrm{p}}^2}\frac{C_{\mathrm{D}}\mathrm{Re}_{\mathrm{p}}}{24}\left(\vec{u}_{\mathrm{p}}-\vec{u}_{\mathrm{c}}\right)+\vec{f}_{\mathrm{other}}\right)\dot{m}_{\mathrm{p}}\Delta t, \tag{4}$$

$$S_{\mathrm{h}} = \dot{m}_{\mathrm{p}}c_{\mathrm{p_p}}\left(T_{\mathrm{p_{in-cell}}} - T_{\mathrm{p_{out-cell}}}\right) \tag{5}$$

where $T_{\mathrm{p_{in-cell}}}$ and $T_{\mathrm{p_{out-cell}}}$ are the particle temperature at the inlet and outlet of each cell.

The Newton's law of motion and the angular momentum equation for a moving particle can be written as follows [35]:

$$\frac{\mathrm{d}\vec{u}_\mathrm{p}}{\mathrm{d}t_\mathrm{p}} = \frac{f_\mathrm{d}}{\tau C_\mathrm{c}}\vec{u}_\mathrm{s} + \vec{f}_\mathrm{B} + \vec{f}_\mathrm{others}, \tag{6}$$

$$I_\mathrm{p}\frac{\mathrm{d}\vec{\omega}_p}{\mathrm{d}t} = \frac{\rho}{2}\left(\frac{d_\mathrm{p}}{2}\right)^5 C_\omega \vec{\Omega}, \tag{7}$$

where u_p, f_d, τ, C_c, u_s, $f_{\mathrm{B}_\mathrm{i}}$, I_p, $\boldsymbol{\omega}_\mathrm{p}$, C_ω and $\boldsymbol{\Omega}$ are nanoparticle velocity, drag function, relaxation time, Cunningham correction factor, particle and fluid relative velocity, Brownian force, moment of inertia, particle angular velocity, rotational drag coefficient and relative particle-liquid angular velocity, respectively. The term $\vec{f}_\mathrm{others}$ includes the other forces.

The general form of Brownian force is presented as [36]:

$$\vec{f}_\mathrm{B} = \vec{\zeta}\sqrt{\frac{6\pi d_\mathrm{p}\mu K_\mathrm{B}T}{m_\mathrm{p}^2\Delta t_\mathrm{p}}}, \tag{8}$$

where $\vec{\zeta}$, d_p, μ, K_B, m_p and Δt_p are random function, particle diameter, viscosity, Boltzmann constant, particle mass and time step, respectively. Since the results of particles migration were not affected by reducing time step lower than 10^{-5}, this value was chosen as time step. The correctness of this form of Brownian force with along the random function is still in doubt [37]. However, two different applicable random functions can be suggested. The first is produced by a Gaussian white noise process; the second is based on a uniform random number, U_i [38]:

$$\zeta_1 = \sqrt{-2\ln U_1}\cos(2\pi U_2), \tag{9}$$

$$\zeta_2 = \sqrt{-2\ln U_1}\sin(2\pi U_2). \tag{10}$$

The potential long-range attractive van der Waals (V_vdw) and repulsion electric double layer (V_EDL) are obtained from DLVO theory [39, 40]:

$$V_\mathrm{vdw} = -\frac{A}{6}\left[\frac{d_\mathrm{p}^2}{2h(h+2d_p)} + \frac{d_\mathrm{p}^2}{2(h+d_\mathrm{p})^2} + \ln\left(\frac{h(h+2d_\mathrm{p})}{(h+d_\mathrm{p})^2}\right)\right], \tag{11}$$

$$V_\mathrm{EDL} = \pi d_\mathrm{p}\varepsilon_0\varepsilon_\mathrm{r}\psi^2\exp(-\kappa h) \quad \kappa d_\mathrm{p} < 10, \tag{12}$$

where ε_0, ε_r, ψ and A are vacuum and relative permittivities, potential on the surface of electrical double layer (approximated by zeta potential) and Hamaker constant, respectively. The Debye–Huckel parameter is obtained for water as $\kappa = 5.6242\times10^{10}\sqrt{I_0/T}$. The value for ionic strength is simply calculated from the general form of $I_0 = \frac{1}{2}\sum_i c_\mathrm{i}z_\mathrm{i}$, the concentration ($c_\mathrm{i}$) based on pH and the charge (z_i) of the species. To avoid immediate aggregation in the solution, the amount of the potential is chosen above isoelectric point of $\psi = -32.0$ mV in this study. Eventually, the combination of the attraction and repulsion will provide the net force as $|F| = \left|\frac{\mathrm{d}V}{\mathrm{d}h}\right|$. Thermophoresis, lift due to shear stress and rotational particle are presented as follows [22, 35, 41]:

$$\vec{f}_\mathrm{thermo} = -\frac{D_\mathrm{T}}{m_\mathrm{p}}\frac{\nabla T}{T}, \tag{13}$$

$$\vec{f}_\mathrm{lift} = 20.3\mu d_\mathrm{p}^2\frac{\vec{u}_\mathrm{s}}{m_\mathrm{p}}\sqrt{\frac{\dot{\gamma}\rho}{\mu}}\mathrm{sgn}(\dot{\gamma}), \tag{14}$$

$$\vec{f}_\mathrm{Magnus} = \frac{1}{2}\frac{A_\mathrm{p}C_\mathrm{ML}\rho}{m_\mathrm{p}}\frac{\left|\vec{u}_\mathrm{s}\right|}{\left|\vec{\Omega}\right|}\left[\vec{u}_\mathrm{s}\times\vec{\Omega}\right], \tag{15}$$

where D_T, $\dot{\gamma}$, A_p and C_ML are thermophoresis diffusion coefficient, shear rate, particle projected area and rotational coefficient, respectively. The important part of the present model is to find a proper drag coefficient for a spherical particle and distorted cluster in the flow. After calculation of distortion factor of a cluster concerning a sphere shape, the drag coefficient can be implemented as:

$$C_\mathrm{D} = \frac{24}{Re_\mathrm{p}}\left(1 + b_1 Re_\mathrm{p}^{b_2}\right) + \frac{b_3 Re_\mathrm{p}}{b_4 + Re_\mathrm{p}}, \tag{16}$$

where b_i are presented by Haider and Levenspiel [42] based on the distortion factor and equivalent diameter of a cluster (proportion of the surface of a spherical particle with the same volume as the actual cluster and surface area of the cluster). A new complete form of heat equation for particles with higher density than water and in nanosize is implemented as follows [43]:

$$m_\mathrm{p}c_{\mathrm{p}_\mathrm{p}}\frac{\mathrm{d}T_\mathrm{p}}{\mathrm{d}t} = m_\mathrm{c}c_{\mathrm{p}_\mathrm{c}}\frac{\mathrm{D}T_\mathrm{c}}{\mathrm{D}t} - 2\pi d_\mathrm{p}k_\mathrm{c}(T_\mathrm{p} - T_\mathrm{c}), \tag{17}$$

where c_p and k are heat capacity and thermal conductivity. The c and p subscripts represent liquid phase (continuous) and particles. The first term on the right is the convective phenomenon induced by flow around the cluster, and the second is conduction occurring on the surface of the cluster with equivalent diameter.

Modelling of cluster formation

To model the aggregation process, two steps should be taken into account, the possibility of the collision and the outcome of the collision. The probability of the collision comes from the ratio of collision volume (two clusters

occupying an equivalent volume) to the total volumetric region.

$$P = \frac{\text{collision volume}}{\text{total volume}} = \frac{\pi(d_{p1} + d_{p2})^2 \left|\vec{u}_s\right| \Delta t_p}{4 \times \text{volume}}. \quad (18)$$

The 1 and 2 subscripts represent smaller and bigger clusters, respectively. The final form of this probability function can be provided based on the possible number of collision n (or the average $\bar{n}$) in each computational domain and Poisson distribution as [44]:

$$P(n) = e^{-\bar{n}} \frac{\bar{n}^n}{n!}. \quad (19)$$

The outcome of the collision should be clearly based on the surface energy on the nanoparticles and tension over the double layer and surrounding fluid. If we assume the random distance between two clusters as $(d_{p1}/2 + d_{p2}/2)\chi^{0.5}$, χ a random number between 0 and 1, and considering the critical offset centre to centre of two clusters as [44]:

$$b_{\text{critical}} = \frac{(d_{p1} + d_{p2})}{2} \sqrt{\min\left(1.0, \frac{2.4f}{We}\right)} \quad (20)$$

where f and We are a function of d_{p1}/d_{p2} and Webber number. Any values smaller than this critical offset will lead to the formation of a cluster, otherwise it is bounced. Determination of surface energy or tension on the double layer of a nanoparticle is the challenging part. The trend of surface tension (microscale) for the mixture of nanofluid is still under question; it may increase [45] or decrease [46]. In nanosize scale, the surface energy density of the nanoparticles is calculated regarding joules per area of the particles containing it. This energy density acts similar to surface tension in macroscale with the same unit. When two particles are about to collide, it can be assumed that they are at their equilibrium distance with the best empirical value of 1.58 ± 0.08 Å [47]. The two important surface energies are van der Waals attraction and EDL repulsion. The former depends on particle diameter and higher than the latter when two particles are at equilibrium distance. However, the total of the surface energy V_{total} will lead to:

$$\gamma = \frac{V_{\text{total}}}{A_p}. \quad (21)$$

γ is the surface energy density of nanoparticles in contact. This is used as the major criterion to understand the final fate of the particles after collision, either bounce or aggregation.

Node-based averaging method

The effects of nanoparticles on parcels in the neighbourhood are not usually applied to the equations. To do this, node-based averaging method is employed to consider the distributing impacts of nanoparticles from the Lagrangian frame into the Eulerian field. The Gaussian distribution function is used to interpolate the neighbouring parcel's impacts on the centroid parcel [48]:

$$\bar{\theta}_{\text{parcel}} = \sum N_{\text{particle}} G_w \theta_{\text{particle}}, \quad (22)$$

$$G_w = \left(\frac{a}{\pi}\right)^{3/2} \exp\left(-a \frac{\left|x_{\text{parcel}} - x_{\text{particle}}\right|^2}{\Delta x^2}\right), \quad (23)$$

$$N_{\text{particle}} = \dot{m}_p \frac{\Delta t}{m_p}, \quad (24)$$

where $\bar{\theta}_{\text{parcel}}$, N_{particle}, G_w, θ_{particle}, Δx, x_{parcel} and x_{particle} are particle variables affected by nodes in the neighbourhood (which are 26 cells for structured quad mesh in this research), number of particles in the parcel, Gaussian weight function, particle variable in the node, characteristic length of the cell, parcel location in the neighbourhood and particle location, respectively.

Numerical procedure

ANSYS-Fluent 17 was employed in this research to solve the governing equations using the control volume approach. The SIMPLE method was used to solve the coupled pressure and velocity in the equations, the QUICK scheme for volume fraction, and the Second-order Upwind for interpolating other parameters. Also, nanoparticles are injected into the flow at the entrance uniformly.

Boundary conditions are uniform velocity and temperature at the inlet for both particles and base fluid (291.15 K as inlet temperature), particle mass flow rate at the inlet calculated based on particle volume fraction up to 0.77 vol% (it is important to make sure particles are uniformly distributed at the inlet), constant heat flux over the external surface of the tube from 69.9 to 108.9 kW/m^2, fully developed condition at the outlet and no-slip condition at the wall of the tube for fluid. It is noted that inlet conditions for particles are equivalent boundary and initial conditions for particles in the Lagrangian frame. Also, wall boundary conditions differ for the particles than base flow. Two main possibilities are that they can either rebound off the wall or stick to the wall. Simulation results showed that none of the mentioned conditions happened for particles. It means that particles never reached the wall or met the wall conditions.

The steps for the computational procedure are as follows:

1. First, the equations of mass, momentum and energy are solved to obtain the flow field variables.
2. The UDF function for extra forces is solved to add to particle motion equation in ANSYS-Fluent 17.
3. The probability of collision and forming a new cluster is considered.
4. The drag coefficient by UDF function is executed regarding new clusters formed.
5. The Newton's law of motion and angular momentum equations are solved.
6. The implemented heat law of the particles is solved to obtain particles temperature.
7. The momentum and heat interactions between fluid and particles are appeared in continuous phase equations as two-way coupling.

Results and discussion

Due to lack of precise study of nanoparticles in convective flows (visualisation and measurements of nanoparticles migration as a discrete and not bulk), the results of heat transfer are validated by the experimental work of Zhang et al. [34], shown in Fig. 2. The good agreement between the predictions and measurements will be the key factor for further predictions of nanoparticles migration. It is noted that the enhancement presented here is concerned with the percentage of increase in heat transfer coefficient for the nanofluid comparing to base fluid.

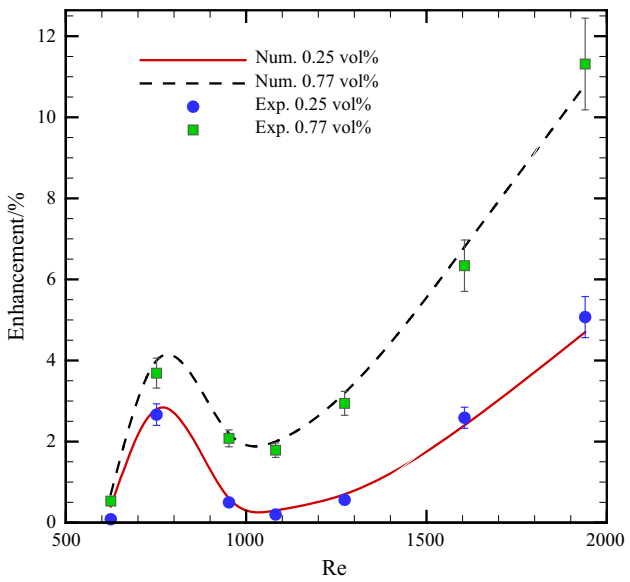

Fig. 2 Comparison between the estimated values by the proposed method and measurements by Zhang et al. [34] for enhanced heat transfer

The growth of nanoparticles cluster is shown in Figs. 3 and 4. The closest radial position to the wall and centre of the microchannel is r = 0.238 mm and r = 0.028 mm, respectively. In fact, the former is placed in the growing part of the convective flow region. As shown in Fig. 3, the majority of the clusters possess the diameter of 20–120 nm, meaning the number of 1–108 nanoparticles in each cluster. The up and down in cluster diameter comes from the joining or leaving of the particles to or from a cluster. Since the aggregation approach used in this research is based on the collisions' probability, particle-to-particle distance plays the key role in final cluster distribution mainly affected by concentration. Hence, a higher concentration in Fig. 3a results in smoother bell curve than the other. All the strong interactions introduced to the particles close to the wall highly influenced particles aggregation at an early stage of residence time in Fig. 4d. The least affected regarding variation in cluster diameter occurs when the nanoparticles are released close to the centreline. It can conclude that the Brownian motion is the dominant force at the centre of the tube in Fig. 4a, which results in less number of collision with other clusters comparing to others near the wall or inside boundary layer at the entrance length.

As previously explained, the cohesion among nanoparticles is caused by the strong van der Waals attraction at equilibrium distance concentred to the aggregation and collision method presented here. The interfacial energy density on the clusters induced by interactions between EDL repulsion and attraction is illustrated in Fig. 5.

The order of magnitude of the energy density is 2×10^{-1} mJ m^{-2} in nanoscale sizes which is almost 100 times smaller than macroscale surface tension of pure water, normally between 0.03 and 0.07 mJ m^{-2}. Due to high dependency of surface energy to nanoparticles diameter, the results are considerably oscillatory. The jump in energy density value is only observed in some parts of clusters close to the microchannel centre in Fig. 5a, because of entering clusters into the convective regions.

The effects of two correlations of the Brownian motion on the particles variables presented in this paper are compared in Fig. 6. The nanoparticles of 20 nm released at injection plan are tracked to calculate both radial and angular displacement. The variation of angular displacement is higher in the case of Brownian motion by Eqs. 9 and 10, but the results of radial movement are more or less the same except for the nanoparticles close to the wall in Fig. 6h. The angular displacements are more distinguished when the nanoparticles are entered into the convective regions in Fig. 6a, b. It is noted that most of the interactions implemented act in radial direction perpendicular to the wall and the difference between two Brownian motion is expected to be more seen in angular displacement. Also,

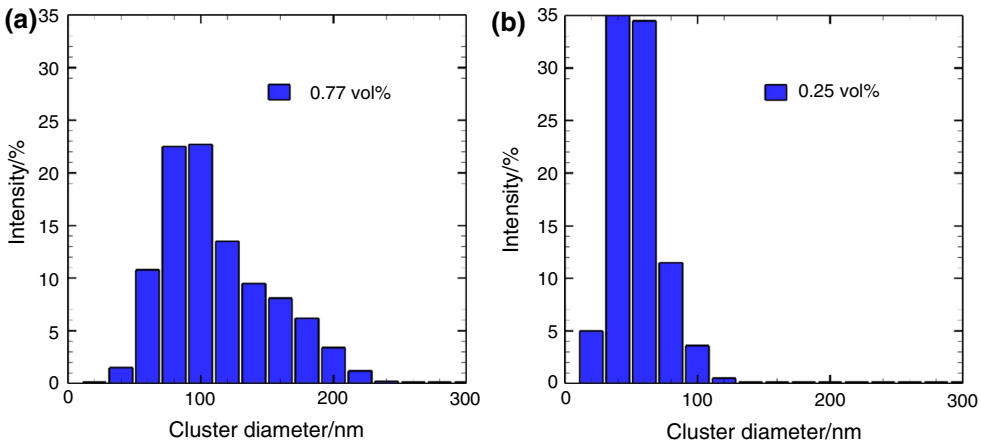

Fig. 3 Statistical distribution of cluster equivalent diameter in the microchannel due to aggregation

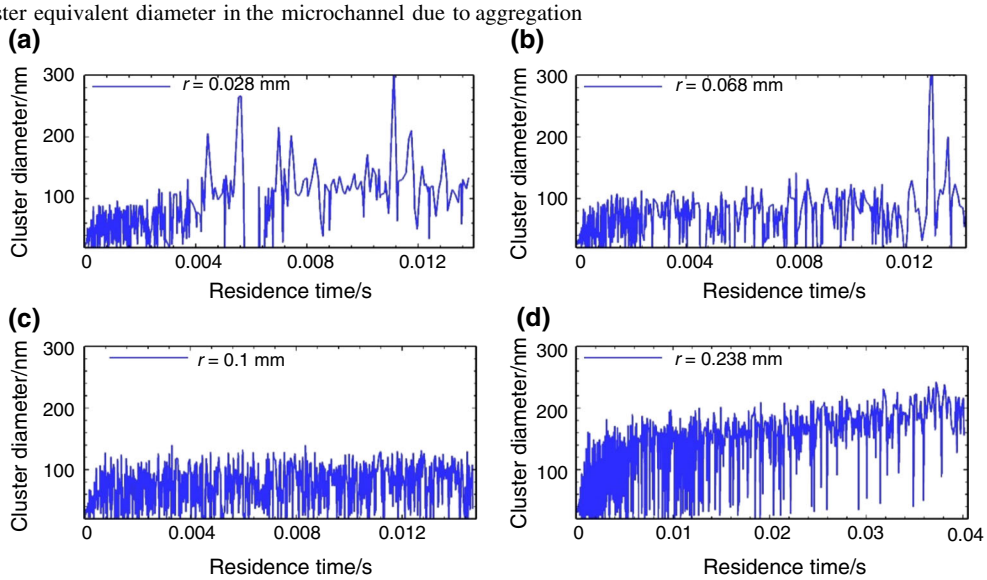

Fig. 4 Aggregation of nanoparticles released from the injected plan at various radial positions (*r* is from the centre of the microchannel)

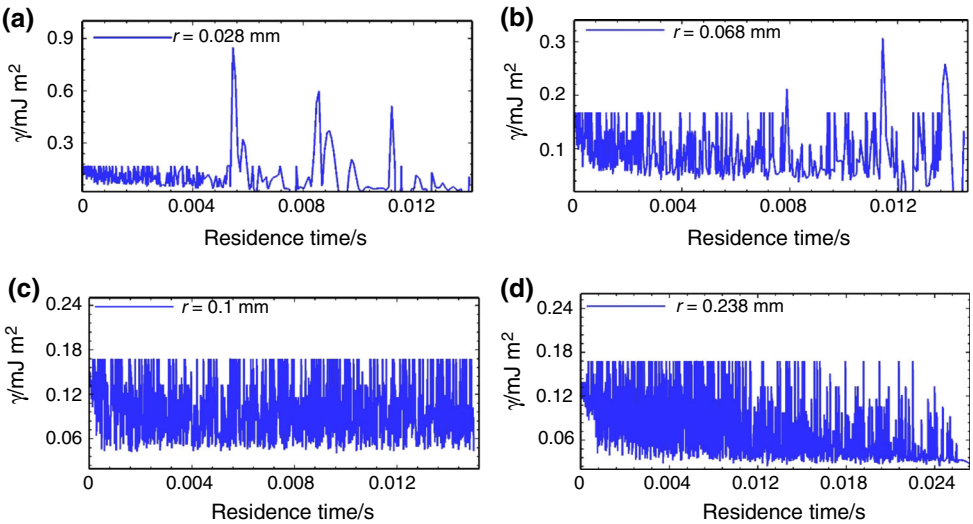

Fig. 5 Surface energy density on the clusters released at different radial locations based on cluster equivalent diameter

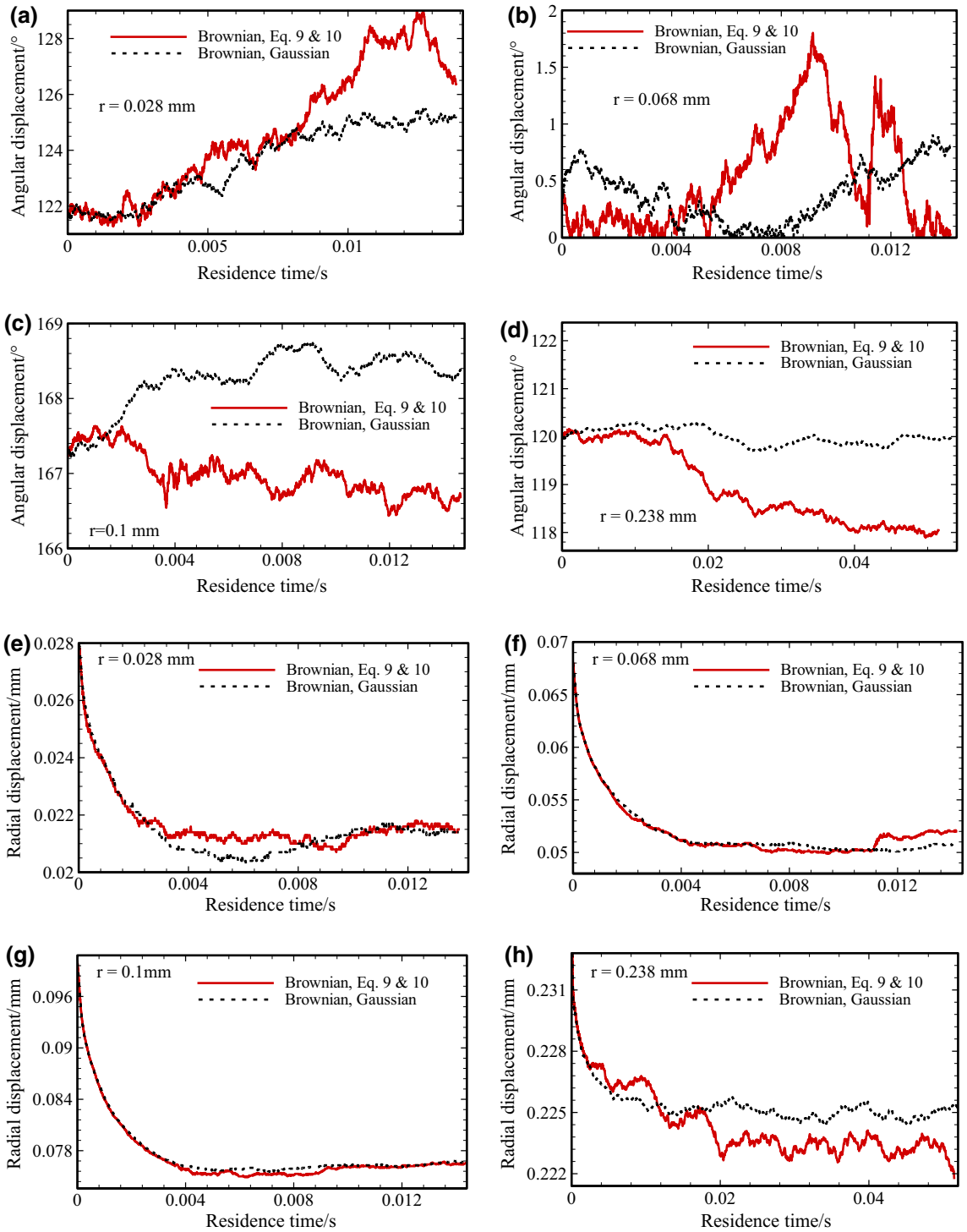

Fig. 6 Migration of nanoparticles in radial and angular direction

the nanoparticles released near the centreline of the tube at r = 0.028 m are mainly influenced by the Brownian force by entering the fully developed section of flow and passing the entrance length, in 0.01 s time which is shown in Fig. 6a. This is caused by the diffusion of the thermal boundary layer into the centreline of the flow, which highly increases the particles vibration and Brownian motion.

Variation of nanoparticles volume fraction from tube inlet to outlet is presented in Fig. 7. X and Y are the cross sections of the tube, and Z is flow direction. Z = 0.001 m is

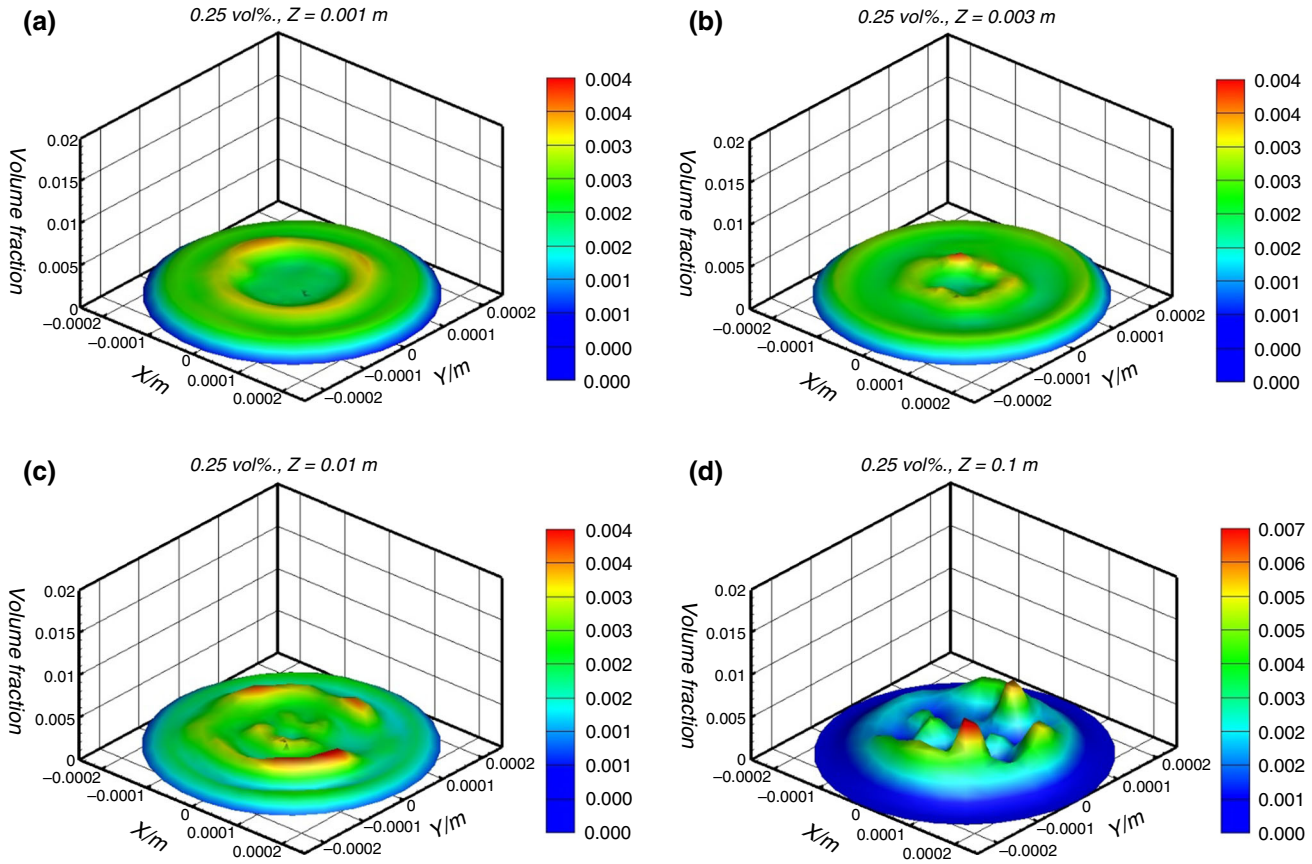

Fig. 7 Evolution of nanoparticles volume fraction from flow entrance (**a**) to outlet (**d**)

still at flow developing section, and higher concentration is depicted at the border of the thermal boundary layer. Due to pushing forces from the wall, nanoparticles tend to be concentrated at the centre of the tube, as the trend shows in downstream until the tube exits at $Z = 0.1$ m. As can be seen, the possibility of forming larger clusters can increase in the middle areas between the wall and centreline because of higher nanoparticles concentration.

Conclusions

In summary, a new method of nanoparticle aggregation was presented, based on the surface energy density defined in this research. Instead of the accumulation of particles in some regions, the probability of the collision was assumed for the surrounding clusters. Therefore, they could leave or join the clusters at the same time, depending on the surface energy. It was found that cluster formation is unavoidable in convective regions and the equivalent diameter distribution turns into a smoother bell curve as the concentration increases. The value for the net surface energy was positive (attraction) at an equal distance, and energy density appeared to be much less than the macroscale surface tension. The impact of specific Brownian random motion is noticeable in the angular displacement of nanoparticles, and proper correlation should be taken into account. This comes from the fact that the particles' migration in radial and angular aspects is directly in charge of mass and energy diffusion and eventually an enhancement in heat transfer. Any changes in particles' angular movement at the centreline are only observed in the thermally fully developed section of the tube due to the interference of thermal diffusion. At the developing section, higher concentration occurs at the edge of the thermal boundary layer due to the pushing forces from the wall. Eventually, the higher volume fraction is found in the area midway between the centreline and the wall.

References

1. Estellé P, Mahian O, Maré T, Öztop HF. Natural convection of CNT water-based nanofluids in a differentially heated square cavity. J Therm Anal Calorim. 2017;128:1765–70.
2. Rashidi S, Mahian O, Languri EM. Applications of nanofluids in condensing and evaporating systems. J Therm Anal Calorim. 2018;131:2027–39.

3. Meibodi SS, Kianifar A, Mahian O, Wongwises S. Second law analysis of a nanofluid-based solar collector using experimental data. J Therm Anal Calorim. 2016;126:617–25.
4. Aberoumand S, Jafarimoghaddam A. Mixed convection heat transfer of nanofluids inside curved tubes: an experimental study. Appl Therm Eng. 2016;108:967–79.
5. Xiao B, Yang Y, Chen L. Developing a novel form of thermal conductivity of nanofluids with Brownian motion effect by means of fractal geometry. Powder Technol. 2013;239:409–14.
6. He Y, Men Y, Zhao Y, Lu H, Ding Y. Numerical investigation into the convective heat transfer of TiO_2 nanofluids flowing through a straight tube under the laminar flow conditions. Appl Therm Eng. 2009;29:1965–72.
7. Esfe MH, Saedodin S, Bahiraei M, Toghraie D, Mahian O, Wongwises S. Thermal conductivity modeling of MgO/EG nanofluids using experimental data and artificial neural network. J Therm Anal Calorim. 2014;118:287–94.
8. Esfe MH, Saedodin S, Mahian O, Wongwises S. Thermal conductivity of Al_2O_3/water nanofluids: measurement, correlation, sensitivity analysis, and comparisons with literature reports. J Therm Anal Calorim. 2014;117:675–81.
9. Yu W, France DM, Timofeeva EV, Singh D, Routbort JL. Thermophysical property-related comparison criteria for nanofluid heat transfer enhancement in turbulent flow. Appl Phys Lett. 2010;96:13–6.
10. Aybar HŞ, Sharifpur M, Azizian MR, Mehrabi M, Meyer JP. A review of thermal conductivity models for nanofluids. Heat Transf Eng. 2014;36:1085–110.
11. Hwang KS, Jang SP, Choi SUS. Flow and convective heat transfer characteristics of water-based Al_2O_3 nanofluids in fully developed laminar flow regime. Int J Heat Mass Transf. 2009;52:193–9.
12. Bianco V, Chiacchio F, Manca O, Nardini S. Numerical investigation of nanofluids forced convection in circular tubes. Appl Therm Eng. 2009;29:3632–42.
13. Kumar N, Puranik BP. Numerical study of convective heat transfer with nanofluids in turbulent flow using a Lagrangian-Eulerian approach. Appl Therm Eng. 2017;111:1674–81.
14. Rashidi S, Bovand M, Esfahani JA, Ahmadi G. Discrete particle model for convective Al_2O_3–water nanofluid around a triangular obstacle. Appl Therm Eng. 2016;100:39–54.
15. Tahir S, Mital M. Numerical investigation of laminar nanofluid developing flow and heat transfer in a circular channel. Appl Therm Eng. 2012;39:8–14.
16. Krishnamurthy S, Bhattacharya P, Phelan PE, Prasher RS. Enhanced mass transport in nanofluids. Nano Lett. 2006;6:419–23.
17. Ganguly S, Sarkar S, Kumar Hota T, Mishra M. Thermally developing combined electroosmotic and pressure-driven flow of nanofluids in a microchannel under the effect of magnetic field. Chem Eng Sci. 2015;126:10–21.
18. Gupta A, Kumar R. Role of Brownian motion on the thermal conductivity enhancement of nanofluids. Appl Phys Lett. 2007;91:223102.
19. Gharagozloo PE, Eaton JK, Goodson KE. Diffusion, aggregation, and the thermal conductivity of nanofluids. Appl Phys Lett. 2008;93:2006–9.
20. Veilleux J, Coulombe S. A dispersion model of enhanced mass diffusion in nanofluids. Chem Eng Sci. 2011;66:2377–84.
21. Putnam SA, Cahill DG. Transport of nanoscale latex spheres in a temperature gradient. Langmuir. 2005;21:5317–23.
22. Eslamian M, Saghir MZ. On thermophoresis modeling in inert nanofluids. Int J Therm Sci. 2014;80:58–64.
23. McNab GS, Meisen A. Thermophoresis in liquids. J Colloid Interface Sci. 1973;44:339–46.
24. Talbot L, Cheng RK, Schefer RW, Willis DR. Thermophoresis of particles in a heated boundary layer. J Fluid Mech. 1980;101:737–58.
25. Koo J, Kleinstreuer C. Laminar nanofluid flow in microheat-sinks. Int J Heat Mass Transf. 2005;48:2652–61.
26. Vladkov M, Barrat JL. Modeling transient absorption and thermal conductivity in a simple nanofluid. Nano Lett. 2006;6:1224–9.
27. Gao JW, Zheng RT, Ohtani H, Zhu DS, Chen G. Experimental investigation of heat conduction mechanisms in nanofluids. Clue on clustering. Nano Lett. 2009;9:4128–32.
28. Babaei H, Keblinski P, Khodadadi JM. A proof for insignificant effect of Brownian motion-induced micro-convection on thermal conductivity of nanofluids by utilizing molecular dynamics simulations. J Appl Phys. 2013;113:084302.
29. Laín S, Sommerfeld M. Numerical calculation of pneumatic conveying in horizontal channels and pipes: detailed analysis of conveying behaviour. Int J Multiph Flow. 2012;39:105–20.
30. Ozturk S, Hassan YA, Ugaz VM. Interfacial complexation explains anomalous diffusion in nanofluids. Nano Lett. 2010;10:665–71.
31. Kumar R, Milanova D. Effect of surface tension on nanotube nanofluids. Appl Phys Lett. 2009;94:073107.
32. Mokhtari Moghari R, Akbarinia A, Shariat M, Talebi F, Laur R. Two phase mixed convection Al_2O_3–water nanofluid flow in an annulus. Int J Multiph Flow. 2011;37:585–95.
33. Yang C, Peng K, Nakayama A, Qiu T. Forced convective transport of alumina–water nano fluid in micro-channels subject to constant heat flux. Chem Eng Sci. 2016;152:311–22.
34. Zhang H, Shao S, Xu H, Tian C. Heat transfer and flow features of Al_2O_3–water nanofluids flowing through a circular microchannel—experimental results and correlations. Appl Therm Eng. 2013;61:86–92.
35. Oesterle B, Dinh TB. Experiments on the lift of a spinning sphere in a range of intermediate Reynolds numbers. Exp Fluids. 1998;25:16–22.
36. Li A, Ahmadi G. Dispersion and deposition of spherical particles from point sources in a turbulent channel flow. Aerosol Sci Technol. 1992;16:209–26.
37. Zhao B, Chen C, Lai ACK. Lagrangian stochastic particle tracking: further discussion. Aerosol Sci Technol. 2011;45:901–2.
38. Box GEP, Muller ME, et al. A note on the generation of random normal deviates. Ann Math Stat. 1958;29:610–1.
39. Marshall JS, Li S. Adhesive particle flow. Cambridge: Cambridge University Press; 2014.
40. Israelachvili JN. Intermolecular and surface forces: revised. 3rd ed. Cambridge: Academic Press; 2011.
41. Zheng X, Silber-Li Z. The influence of Saffman lift force on nanoparticle concentration distribution near a wall. Appl Phys Lett. 2009;95:24–7.
42. Haider A, Levenspiel O. Drag coefficient and terminal velocity of spherical and nonspherical particles. Powder Technol. 1989;58:63–70.
43. Michaelides EE, Feng Z. Heat transfer from a rigid sphere in a nonuniform flow and temperature field. Int J Heat Mass Transf. 1994;37:2069–76.
44. O'Rourke PJ. Collective drop effects on vaporizing liquid sprays. Los Alamos Natl Lab, NM. Technical report; 1981.
45. Bhuiyan MHU, Saidur R, Amalina MA, Mostafizur RM, Islam A. Effect of nanoparticles concentration and their sizes on surface tension of nanofluids. Proc Eng. 2015;105:431–7.
46. Chinnam J, Das DK, Vajjha RS, Satti JR. Measurements of the surface tension of nanofluids and development of a new correlation. Int J Therm Sci. 2015;98:68–80.

47. Van Oss CJ, Chaudhury MK, Good RJ. Interfacial Lifshitz-van der Waals and polar interactions in macroscopic systems. Chem Rev. 1988;88:927–41.

48. Apte SV, Mahesh K, Lundgren T. Accounting for finite-size effects in simulations of disperse particle-laden flows. Int J Multiph Flow. 2008;34:260–71.